TD-99-037
August 3, 1999

Study of Saturation Effect in 43.5-mm High Field Dipole Magnet Design

J. Moeller, T. Lee, & R. Yamada
Fermilab, Batavia, IL - 60510

Summary

The purpose of this note is to report results on the study of iron saturation effects in the 43.5-mm design for a high field dipole magnet [1]. Previously, similar studies of this nature have been conducted and reported for 45- and 50-mm designs [2]. The procedural details on using ANSYS for such studies are outlined in a separate paper [3]. In the first part of this paper, we discuss our efforts to optimize the saturation-induced harmonics using yoke holes, other important field calculations, and improved methods for approximating the current distributions in the dipole. In the last part of this paper, these methods are applied to the finalized yoke geometry and the results are reported.

1. Introduction

As the excitation current increases, the field distribution in the beam bore becomes increasingly distorted due to the saturation of the yoke. Usually, the sextupole term suddenly has a positive increase when the top and bottom inner yoke surfaces reach about 2.0 T [2]. Around the circular surface of the iron, the top and bottom regions become more saturated than the side regions. Because the saturation pattern is non-uniform around the inner surface of the yoke iron, a positive sextupole component is added to the field. This trend continues with increased excitation and the sextupole term peaks when the side iron starts to saturate around 2.0 T. With further increase in yoke saturation, the sextupole term gradually decreases beyond this peak. This behavior is more prominent in designs with less space between the coil and the inner surface of the iron yoke. During this cycle of operation, the other higher harmonics remain fairly small and constant [4].

2. Application of Holes in Yoke for the Correction of Iron Saturation Effect

The use of holes in the yoke for the correction of iron saturation has been tried and used with superconducting magnets in the past. Its application to the RHIC magnets was reportedly a success [5]. In this case, the central field was up to 3.46 T. The holes were also applied in our design study of the 50-mm and 45-mm bore dipoles for 11 to 12 T field [2,4]. In such designs, the holes are introduced near the side surfaces of the yoke so that the inner iron starts to saturate at the side surfaces earlier than in the case without the holes. By trying to make the whole iron surface saturate more uniformly with the proper distribution of holes, we can reduce the magnitude of the sextupole term. We conducted this study with a 43.5-mm bore magnet design using ANSYS.

3. Programming Procedure

The studies were performed using the Finite Element program ANSYS [3]. Two-dimensional electromagnetic models were constructed using ROXIE-derived coil cross-sections. Throughout this study, the inner and outer radii of the iron yoke were held fixed at 60 mm and 200 mm, respectively, as originally designed [1]. The distance between the coil and the inner radius of the yoke is ~8.0 mm. Magnetic field calculations were first done with a solid iron yoke for comparison to other iron configurations. Magnet excitation was simulated at several key current values for each iron configuration. For each run, the solid iron configuration was modified by introducing one or more circular holes filled with a vacuum element. A solution routine was executed with load steps of various currents. The harmonic field components were then extracted in a two-step process. The radial field component, B_r, was first extracted at 49 equally spaced points on a 1-cm radius using an ANSYS path operation. This data was then processed by the harmonic analysis routine TRICOF that was extracted from the program ROXIE [3]. The resulting harmonic data was then graphed versus current and analyzed. Flux line and flux density plots were also obtained to aid our understanding of the holes' re-routing effect on flux density. By correlating changes in the shape of the sextupole vs. current curve to placement of holes in the iron, we were able to reduce the sextupole presence by strategically configuring the yoke holes.

4. Optimization of Saturation-Induced Harmonics Using Holes in Yoke

In strategically configuring the holes in the iron yoke for the 43.5-mm bore, we decided that the best approach was to use a geometry that was similar to the optimized 45-mm design [4]. We did this by creating two holes and one semicircle in the same locations as the 45-mm design. The geometry and flux density pattern is shown in Figure 1. Our first experimentation involved creating the first hole (d1) with a 30-mm diameter, the second hole (d2) with a similar diameter, and the semicircle (d3) with a 20-mm diameter. According to the results of the ANSYS magnetic simulation, we were able to reduce the peak value sextupole harmonic of the solid iron from about 5.5 units to about 3 units, as shown in Figure 2. Next, we decided to decrease the diameter of the second hole (d2) to 20-mm. This resulted in the reduction of the peak sextupole harmonic value to about 1.2 units. Unfortunately, the minimum harmonic for this run dipped drastically to about -4 units. To better balance the sextupole harmonic, an intermediate 25-mm (d2) hole was created. The simulation produced a peak sextupole value of 2.2 units, and a minimum value of about -2.9 units. Figure 2 compares the sextupole reduction of the different configurations. Although these runs did not produce a fully-optimized design, it set the foundation for our knowledge of the effects of hole configurations and the reduction of the sextupole harmonic for future designs. At this point, we stuck with the best design which had d2=25 mm for all subsequent calculations.

5. Other Field Calculations

Continuing on with the semi-optimized design of d1=30, d2=25, and d3=20 mm, we next analyzed field data. Figure 3 compares central and peak field load lines with original ROXIE results. The peak values are about 4.6% higher than the central field values in this region. The ROXIE central field data correspond to the case without any saturation effects due to the iron. The short-sample cable data are included at various degrees of degradation so that one can deduce quench field values by tracing the intersection of S.S. data and peak field straight down to the central field curve. The short sample curves correspond to an I_c value of 800 A at 12 T with 28 strands in the cable. Without any degradation in the cable the central field will be 11.6 T, and with 20% degradation it will be 11.0 T. It is interesting to note that by the cable degradation of 20% in I_c current, the maximum obtainable field value is reduced by only 5%.

Fringe field measurements are one of the key factors for equipment and safety of a good magnet design. We took the 43.5-mm design and extended the universe (air) to a length of 40-cm beyond the outer surface of the iron yoke. Using ANSYS, we calculated the vertical component of the field in this 40-cm wide outer space. Figure 4 shows our results, with a fringing field at the edge of the iron of approximately 900 Gauss at 18 kA, and 1.3 kilo-Gauss at 20 kA. Along with this field calculation, we proceeded to calculate the field in the iron midplane of the same design. Figure 5 shows these results with a dip occurring at about 1.5-cm to 3.5-cm as a result of the 20-mm semicircle hole.

6. Improvements in Current Distribution Approximation

In pursuing these studies, it was observed that there was an unexplained positive sextupole component of about 0.5 units at low current and low field. This value was not present in comparable ROXIE analyses, so we decided to find out what was causing it. Upon reviewing the method that ROXIE uses to approximate the current distribution in the conductor turns, we determined that the method we were using in ANSYS for this was not comparable to ROXIE's. Our method assigned a constant current density to the entire trapezoidal cross-sectional area of each turn, whereas the method used by ROXIE accounted for minute changes in current density due to individual strands and the keystoning of the cable. This difference in the two methods was hypothesized as being the reason for the disparity in the low-field sextupole component.

We next devised a new method for assigning currents in ANSYS that would better approximate the distribution of currents within the individual conductor turns. Each conductor turn was subdivided into a 2x14 matrix of elements that approximated the 28-strand makeup of the cable. The 28 elements varied in cross-sectional area due to the keystoned geometry of the cable and did not contain any gaps between strands. Regardless of these non-ideal constraints, we felt that this new geometry would suffice as a better approximation of the conductor. We next went about the task of individually assigning current densities to each of the newly defined conductor sub-elements. A macro was used to run through each sub-element and assign to it a current density equal to the nominal current divided by the cross-sectional area of that particular sub-element. Since the areas of the sub-elements varied across each turn due to the keystoning, this produced a corresponding variance in the distribution of current density. The ±6%

deviation of thickness at the ends from the mid-thickness in the cable accounted for an exactly ±6% deviation in the current density in the ends from the centroid value. A graphical representation of this is shown in Figure 6.

Using this new approximation of the current density in the conductors, we were able to attain better agreement with ROXIE data for the low field sextupole. But this does not necessarily mean that there is agreement between the calculations and real-world data. Figure 7 compares results from runs with and without yoke holes using both the new and old methods of distributing current density. The 0.5 unit of sextupole that had existed below 8000 A in the old runs has been reduced to effectively 0 units. Lastly, Figure 8 shows all pertinent harmonics for the optimized hole pattern using the new current distribution.

7. Second Case Study With Finalized Yoke Design

Our second case study contained a finalized design for the iron yoke, which still had the same inner and outer iron radii of 60 and 200 mm, respectively. The size of the notch at the inner surface was increased to 3-mm wide by 2-mm high. We changed the locations and sizes of the clamp slots and notches. Along with that, we also reconfigured the holes. With these changes, we were able to run four simulations that produced similar results to the first case study. Our most optimized result is shown in Figure 9. Here, the locations and sizes of the holes were different from the first case study. Using Figure 9 as a reference, the diameter of the first hole (d1) is 40mm, the second hole (d2) is 24.6mm, and the semi-circle (d3) is 28mm. In Figure 10, the magnetic flux line distribution is shown for the case with the finalized yoke design at 18 kA excitation current and 10 T central field.

The sextupole harmonics for this optimized design are graphed with runs of other configurations, as shown by Figure 11. This design (shown in red with cross marks), although not fully optimized, is the best out of the four runs because the positive and negative sextupole harmonics are somewhat symmetric. According to Figure 11, the sextupole peaks at about 2 units and dips down to a minimum of only –3 units.

In Figure 12, all harmonics from b_3 to b_{13} are shown for the case with the finalized yoke design with the optimized configuration of the holes. All harmonics except b_3 are within ±0.3 units for the whole range of excitation current. The reconstructed field distribution in the beam bore on the median plane is shown in Figure 13. The field variation is within ±0.0005 units up to the radius of 1.25 cm. This field swing is due to the sextupole term b_3.

Using our most updated design, we extracted some useful data that would help us to understand the ways in which we could further reduce the sextupole. For example, we extracted the magnetic field values at the specific regions (0°, 22°, 90°) of the inner iron, and we plotted these results with the sextupole as shown in Figure 14. As can be seen in this graph, the sextupole term starts to rise when the top part of the inner surface of the yoke goes above 2 T. And when the inner surface at 0° (mid-plane) goes above 2 T, the sextupole peaks and then starts to decrease.

In order to understand the magnetic flux density distribution inside the yoke, we plotted the azimuthal flux density at 5-mm offset from the inner radius of the iron. This distribution is shown in Figures 15 and 16 for the cases with the finalized yoke geometry

with and without holes. Figure 15, with the optimized holes, shows a much more uniform distribution over the angle compared to Figure 16 without holes. We can clearly see the effect of holes, which raise the saturation level of the magnetic flux at smaller angles above the 7.5 kA excitation level.

References

[1]. V. Kashikhin, "First High Field Magnet Cross-Section Design." TD-99-027, 6/7/99.
[2]. R. Yamada & J. Moeller, "Saturation Effect and Field Correction Using Holes in Yoke." TD-99-017, March 1999.
[3]. J. Moeller, "ANSYS Procedure for 2D Field Analysis and Iron Saturation Study." TD-99-016, March 1999.
[4]. R. Yamada, J. Moeller, and M. Wake, "Design Study of 45-mm Bore Dipole Magnet for 11 to 12 Tesla Field." TD-99-012. March 26, 1999.
[5]. R. Gupta, "Improving the Design and Analysis of Superconducting Magnets for Particle Accelerators." Thesis. November 1996.
[6]. S. Russenchuck, "ROXIE : A Computer Program for the Design of Superconducting Accelerator Magnets." CERN AT/95-39, LHC Note 354, September 26, 1995.

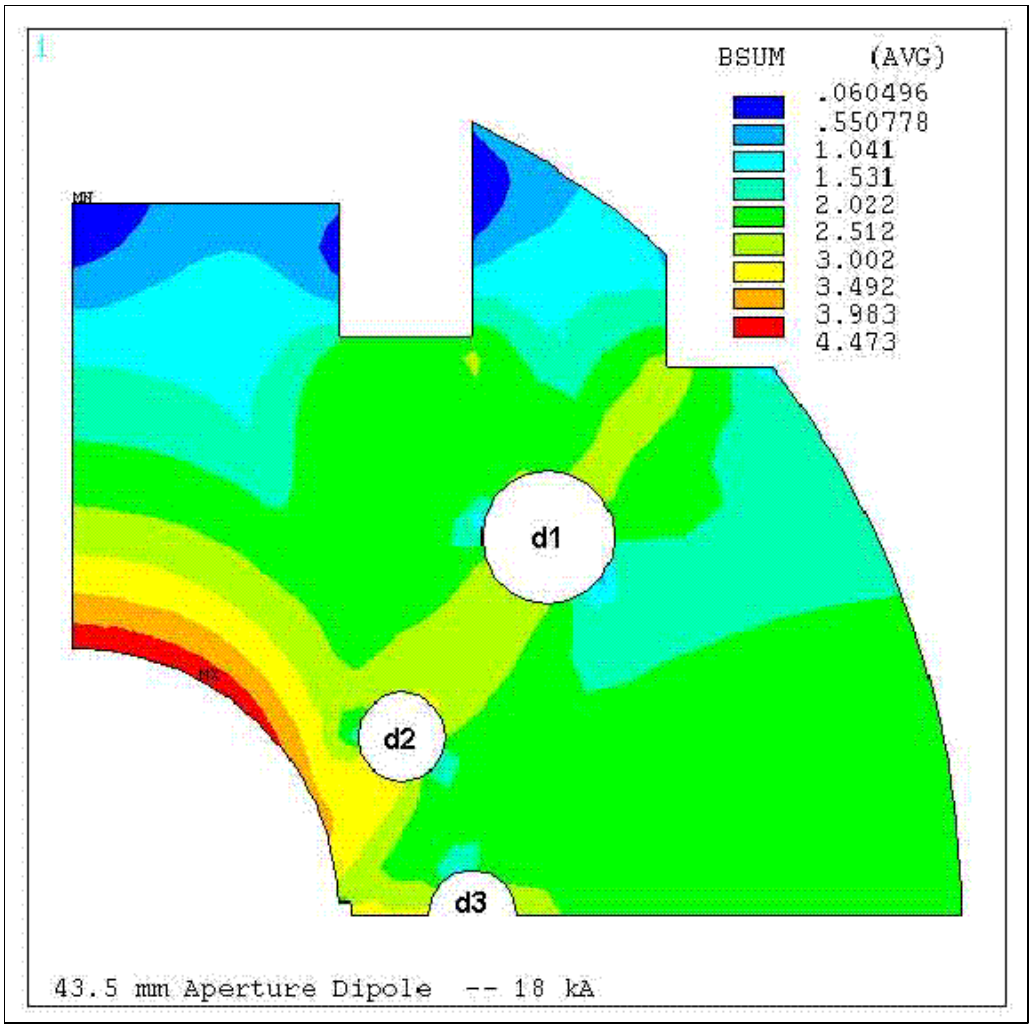

Figure 1. Geometry and associated flux density distribution of iron yoke. (d1=30 mm, d2=20 mm, d3=20 mm)

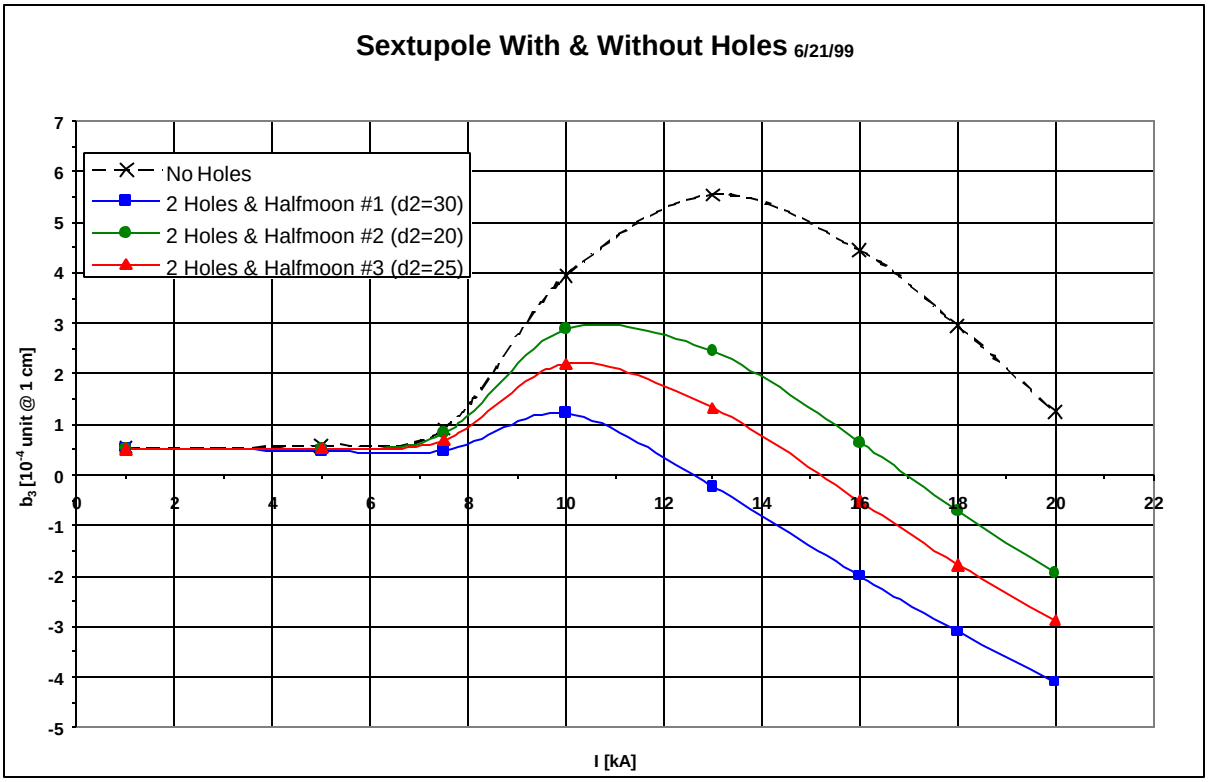

Figure 2. Comparison of sextupole variation in several iron yoke hole configurations.

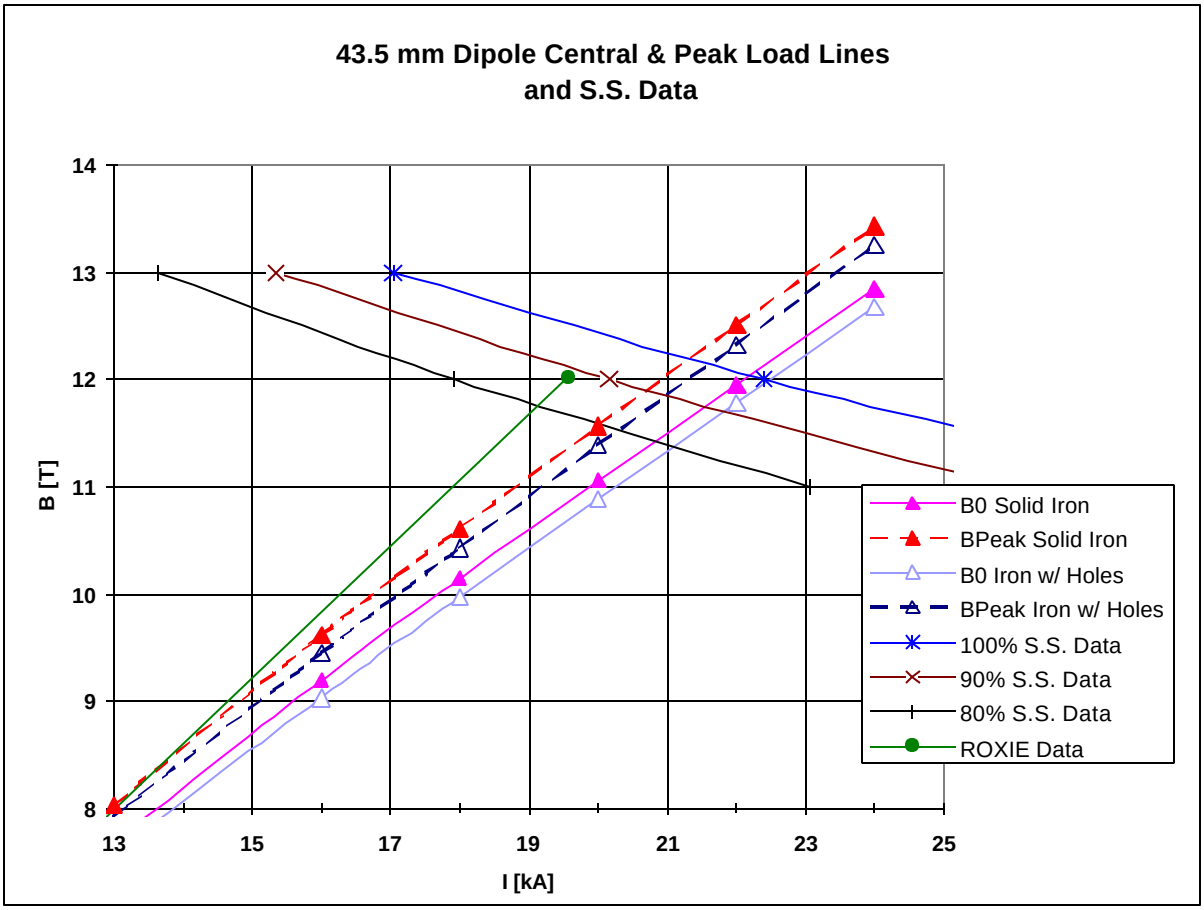

Figure 3. Central and peak load lines and associated short sample data (with d1=30, d2=25, d3=20 mm hole configuration).

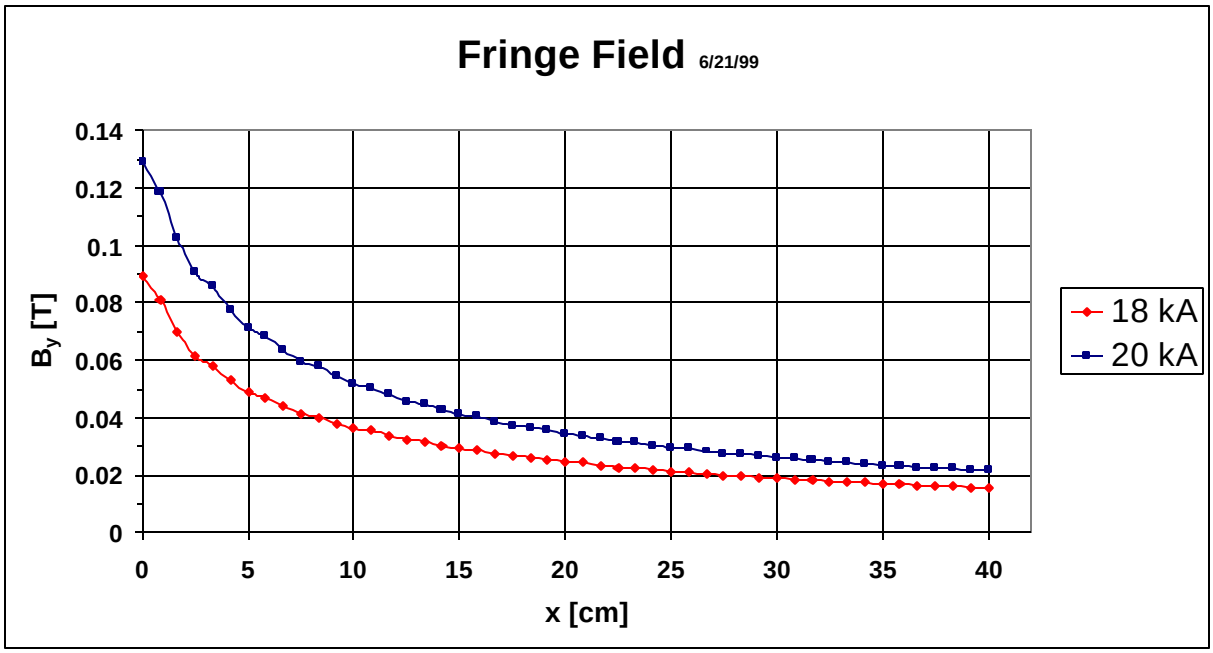

Figure 4. Fringe field from outer edge of iron out to 40 cm. (with d1=30, d2=25, d3=20 mm hole configuration).

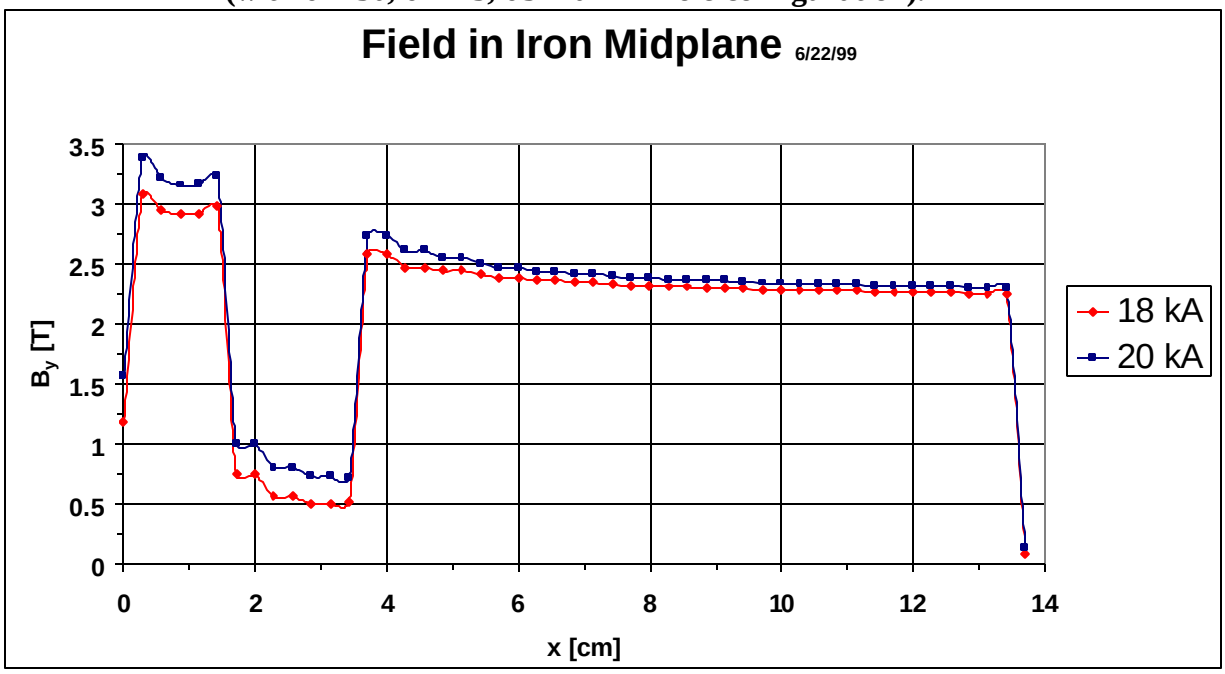

Figure 5. Vertical component of field on midplane of iron yoke. (with d1=30, d2=25, d3=20 mm hole configuration).

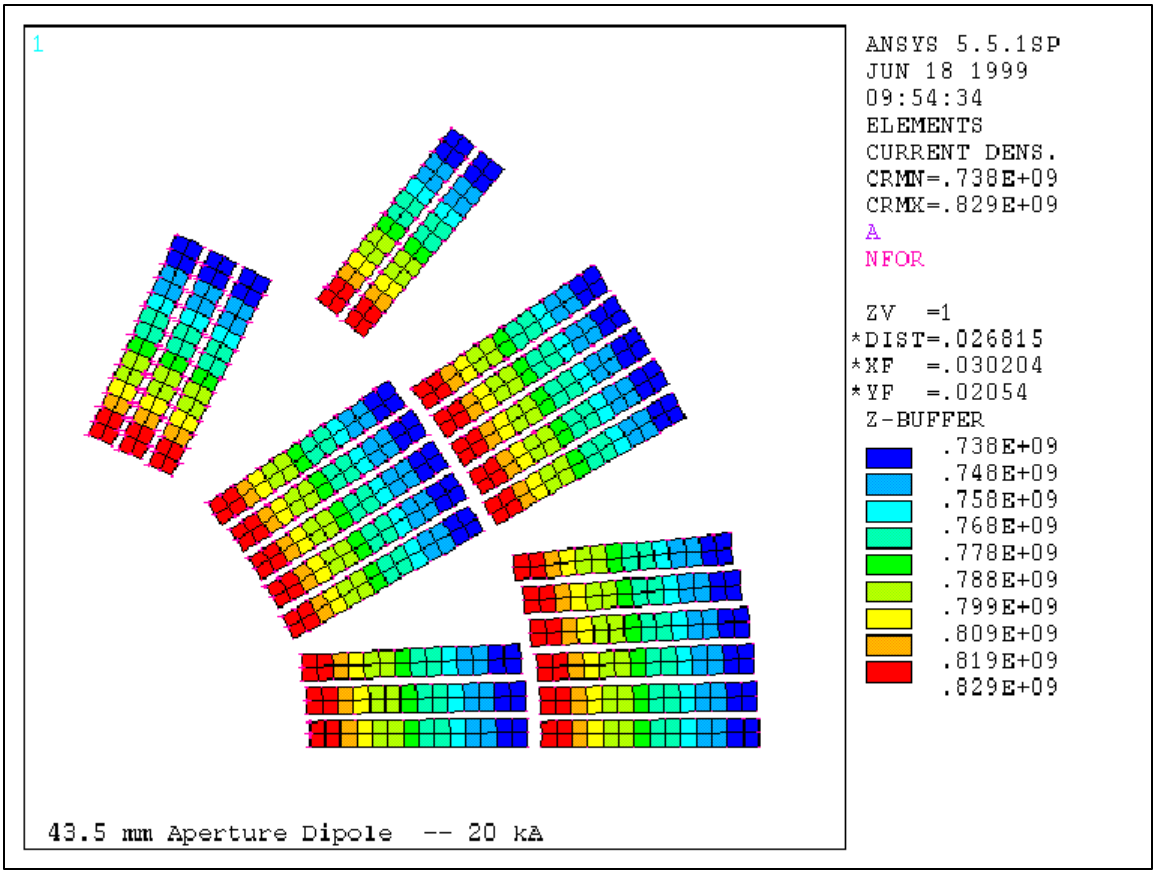

Figure 6. Improved current density distribution in coil turns.

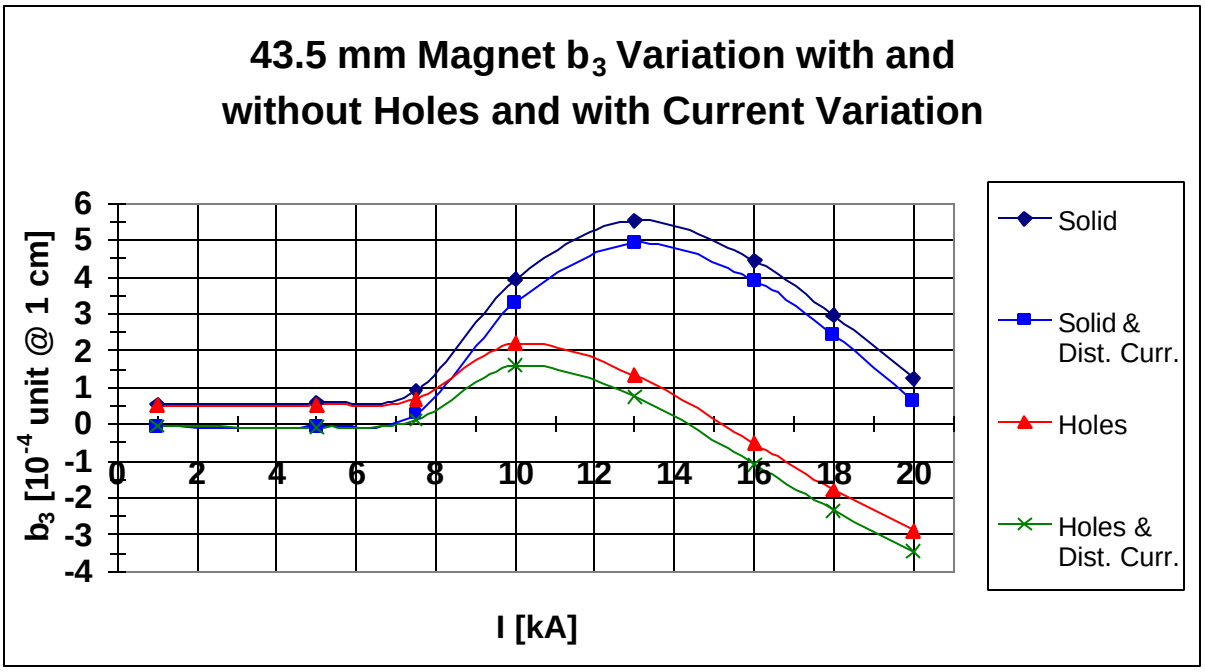

Figure 7. Comparison between sextupole term calculations with and without improved current density distribution. (d1=30 mm, d2=25 mm, d3=20 mm)

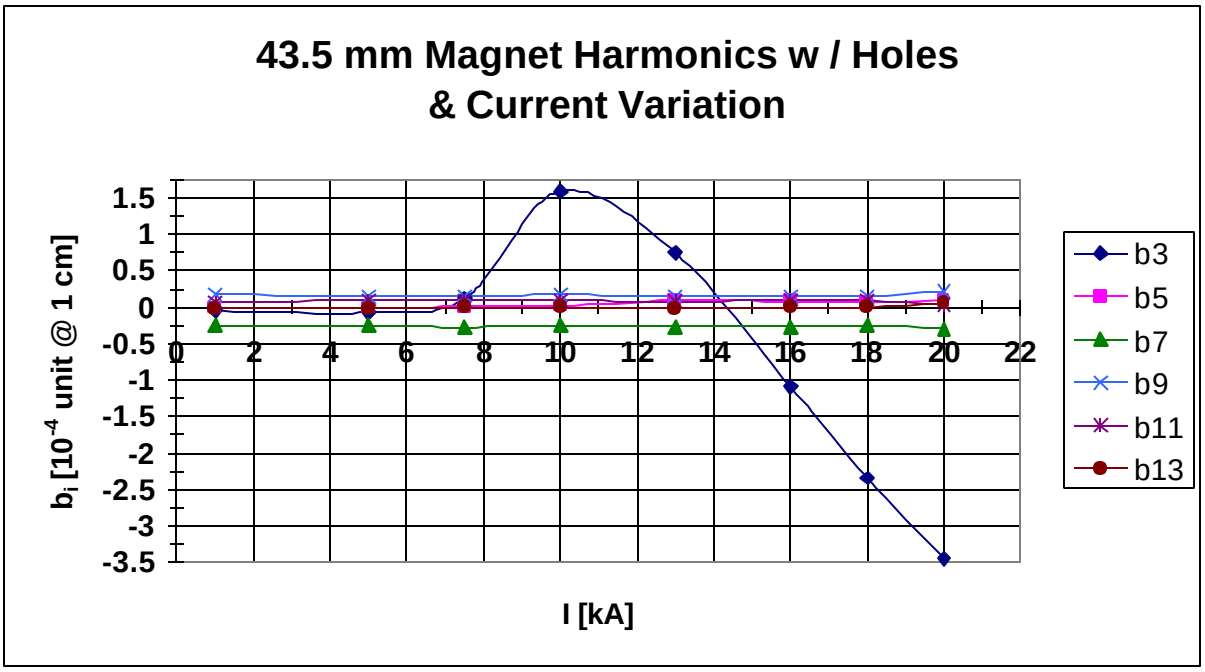

Figure 8. Harmonics of optimized-hole geometry using improved current density distribution. (d1=30 mm, d2=25 mm, d3=20 mm)

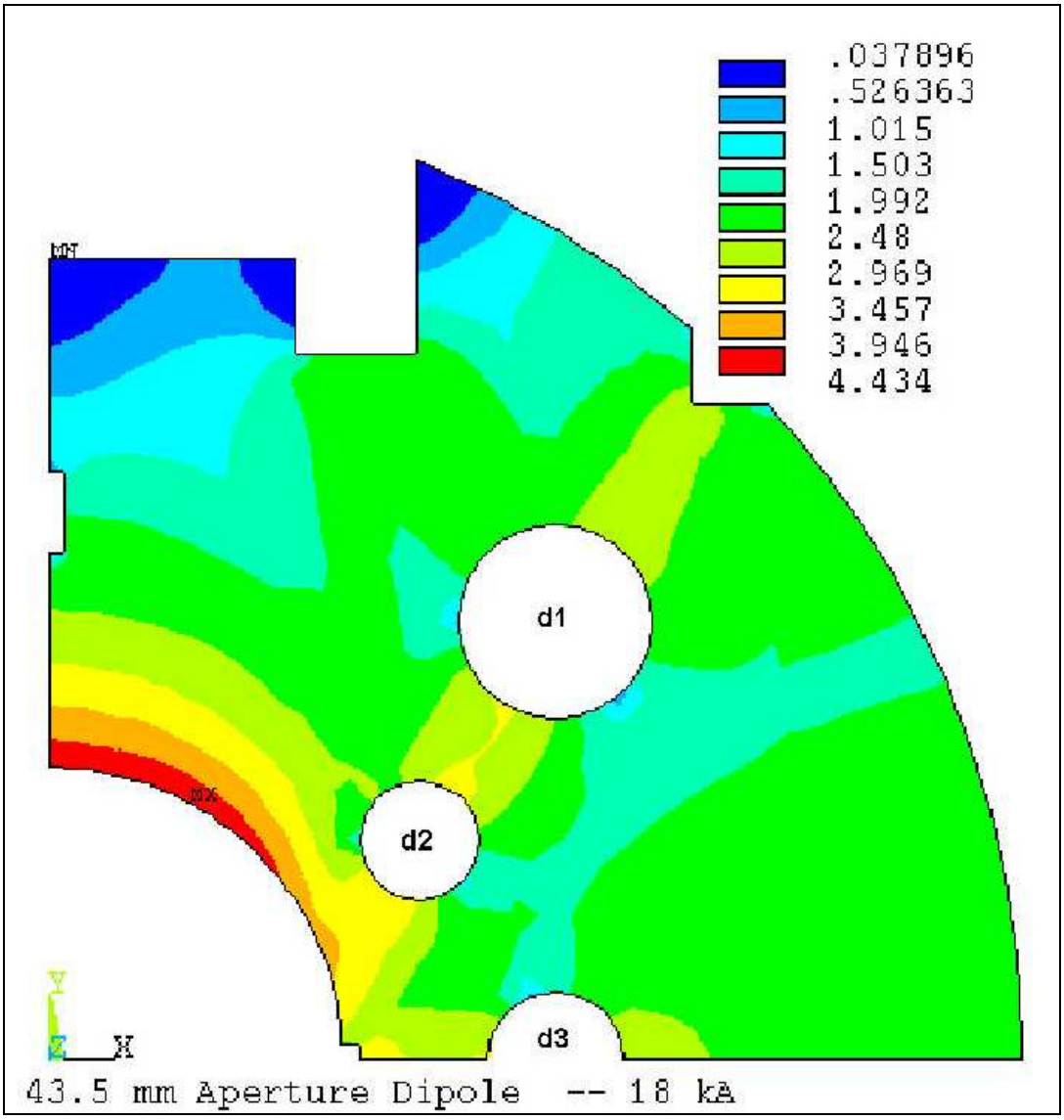

Figure 9. Geometry and associated flux density distribution of the finalized yoke design at 18 kA and 10 T central field. (d1=40 mm, d2=24.6 mm, d3=28 mm)

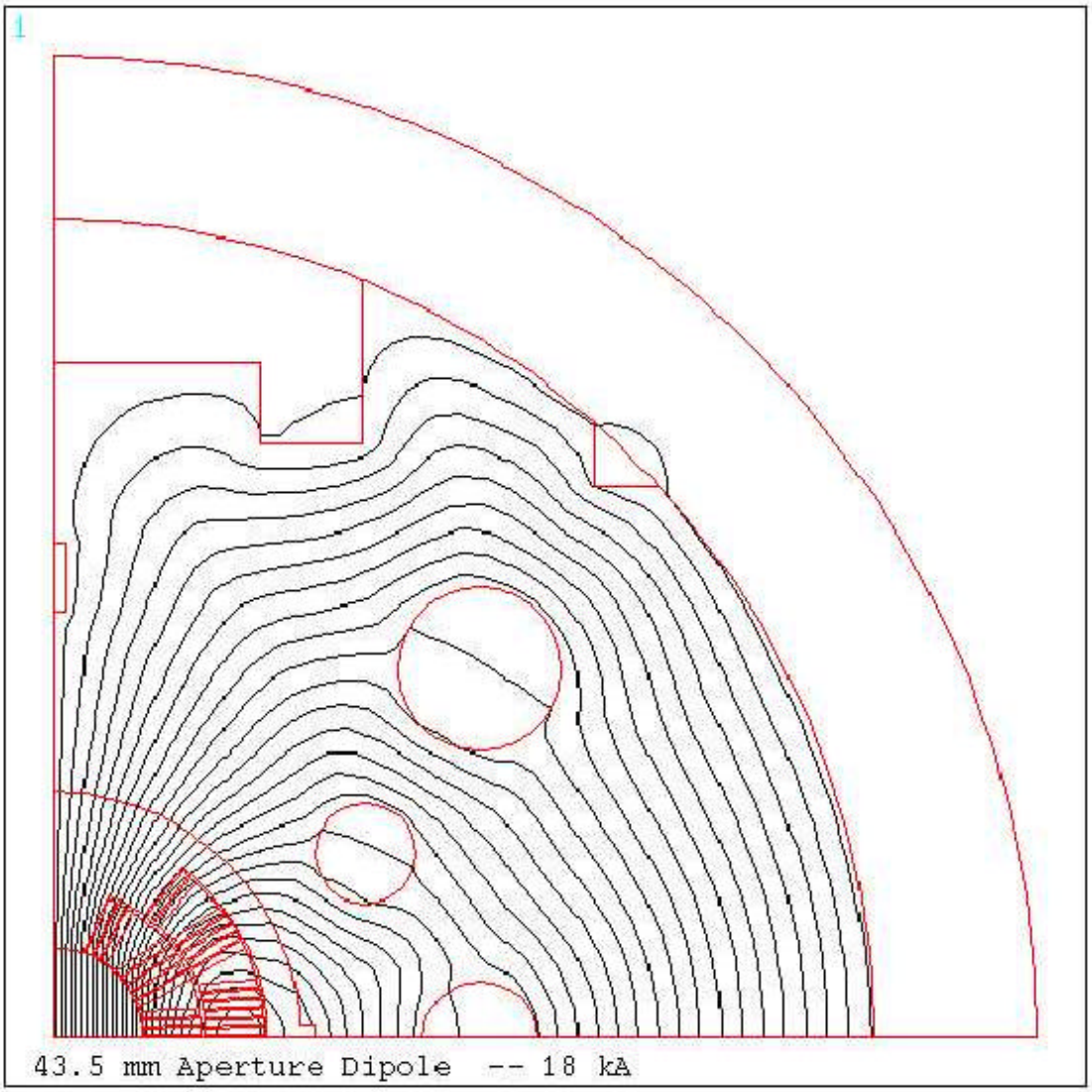

Figure 10. Flux line distribution inside the finalized yoke design at 18 kA and 10 T central field.

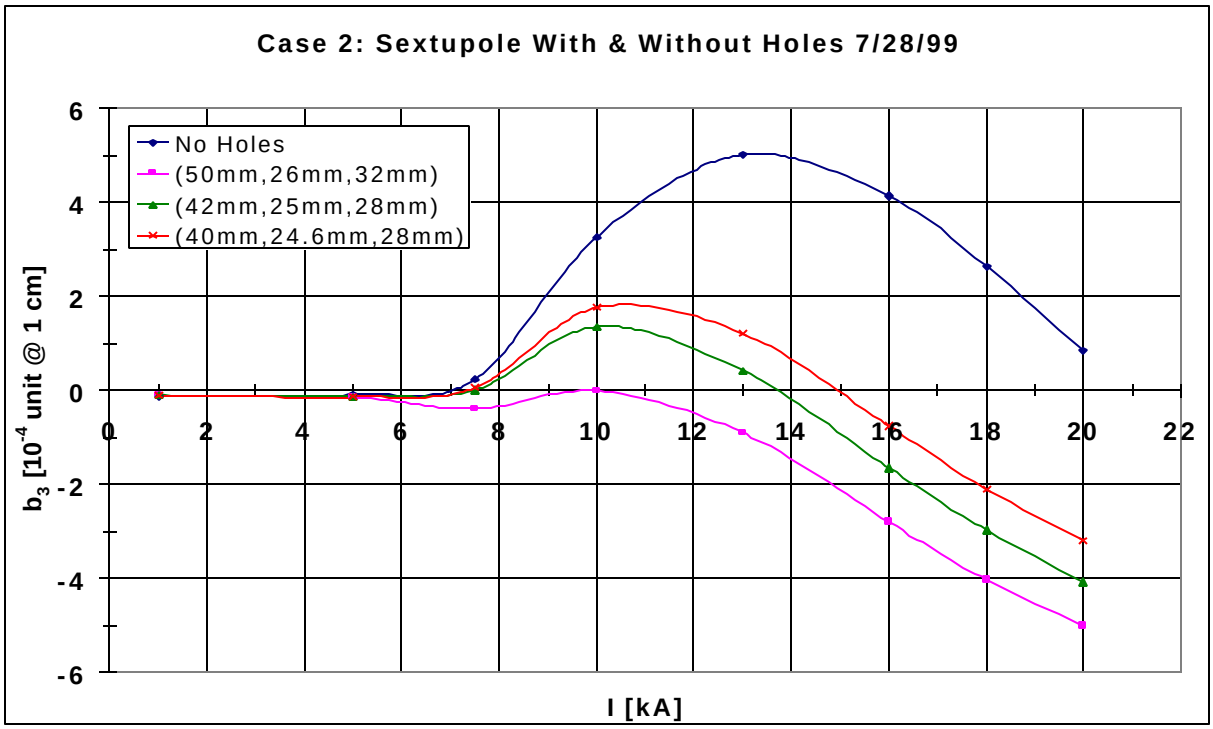

Figure 11. Comparison of sextupole variation in several iron yoke hole configurations with the finalized yoke design.

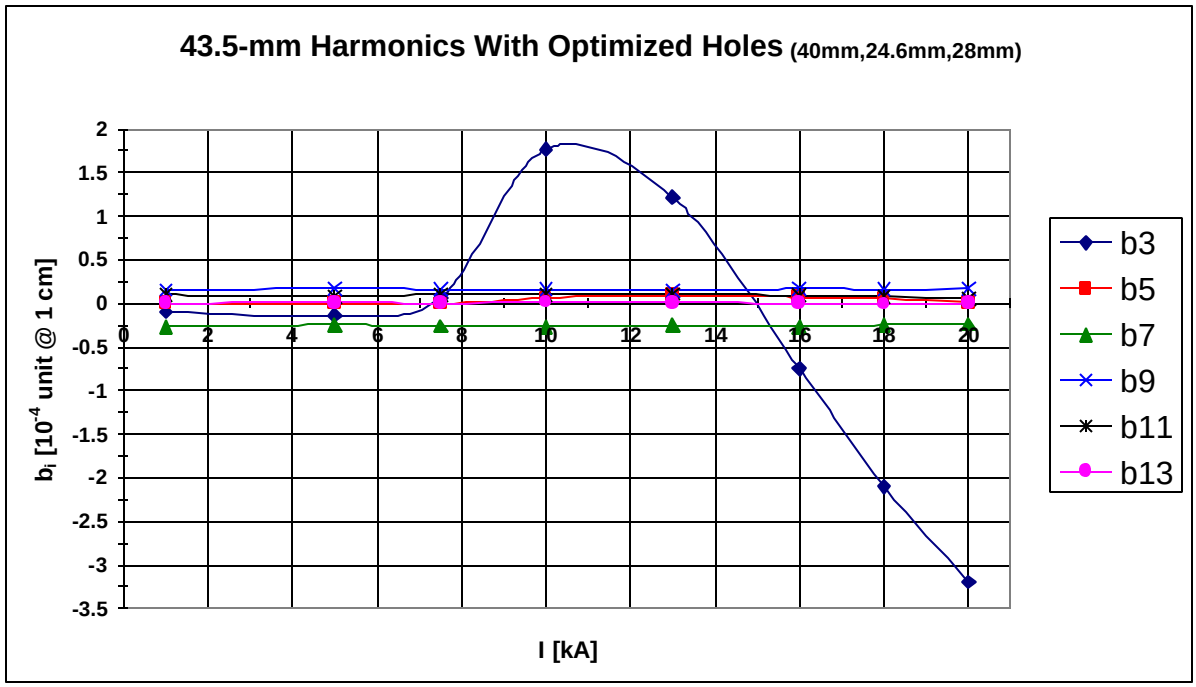

Figure 12. Harmonics of finalized yoke design with optimized hole configuration. (d1=40 mm, d2=24.6 mm, d3=28 mm).

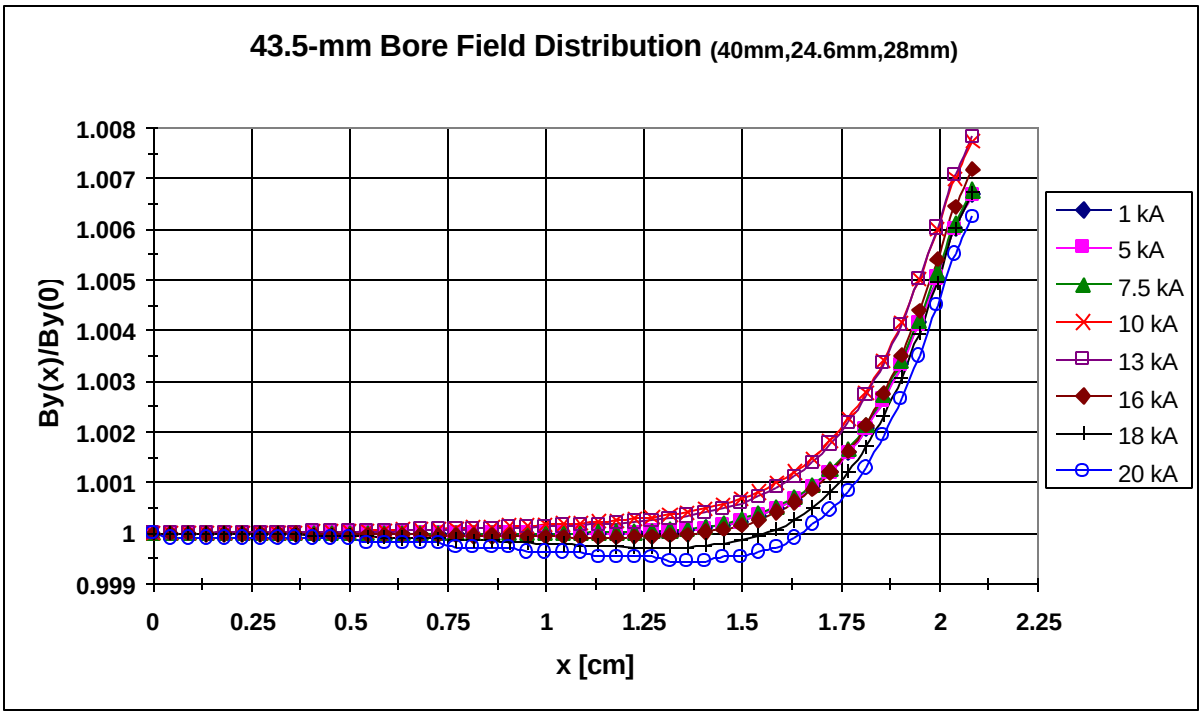

Figure 13. Reconstructed field distribution in the beam bore from 1 kA to 20 kA.

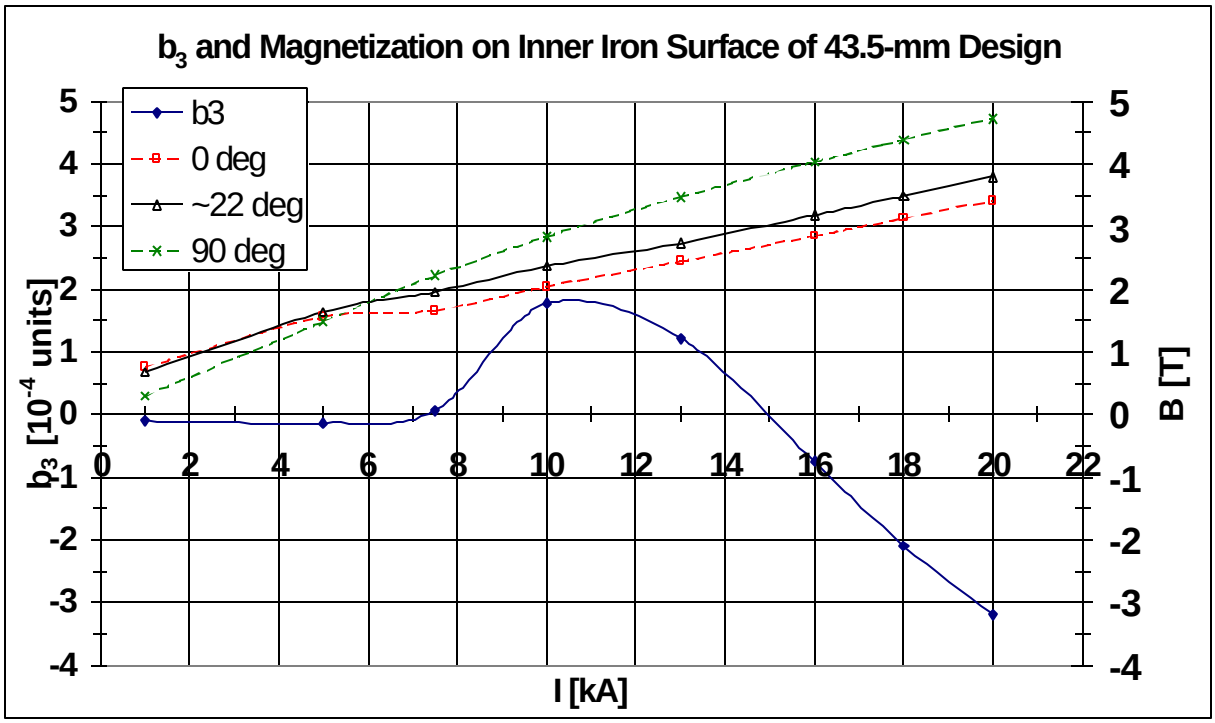

Figure 14. Sextupole plotted with field at 0°,22°, and 90° locations on inner iron surface for best-case hole configuration with the finalized yoke design. (d1=40 mm, d2=24.6 mm, d3=28 mm)

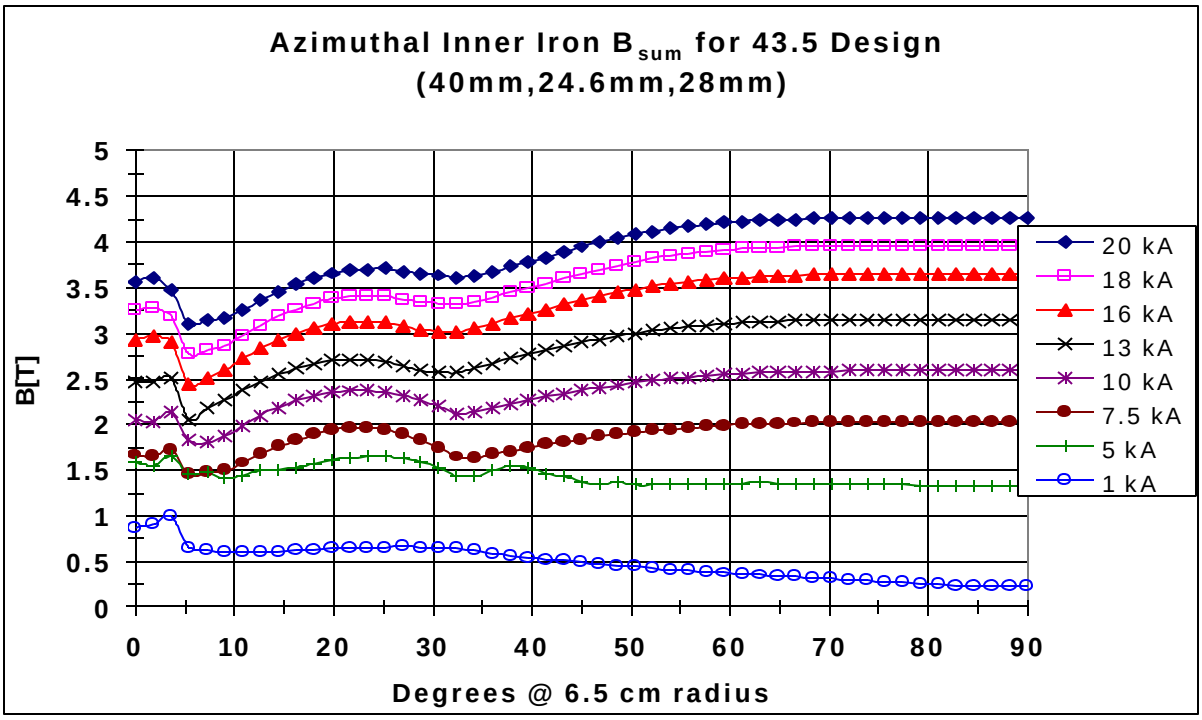

Figure 15. Magnetic flux density distribution taken azimuthally at 5-mm offset from inner radius of iron yoke for the finalized yoke design with optimized hole configuration.

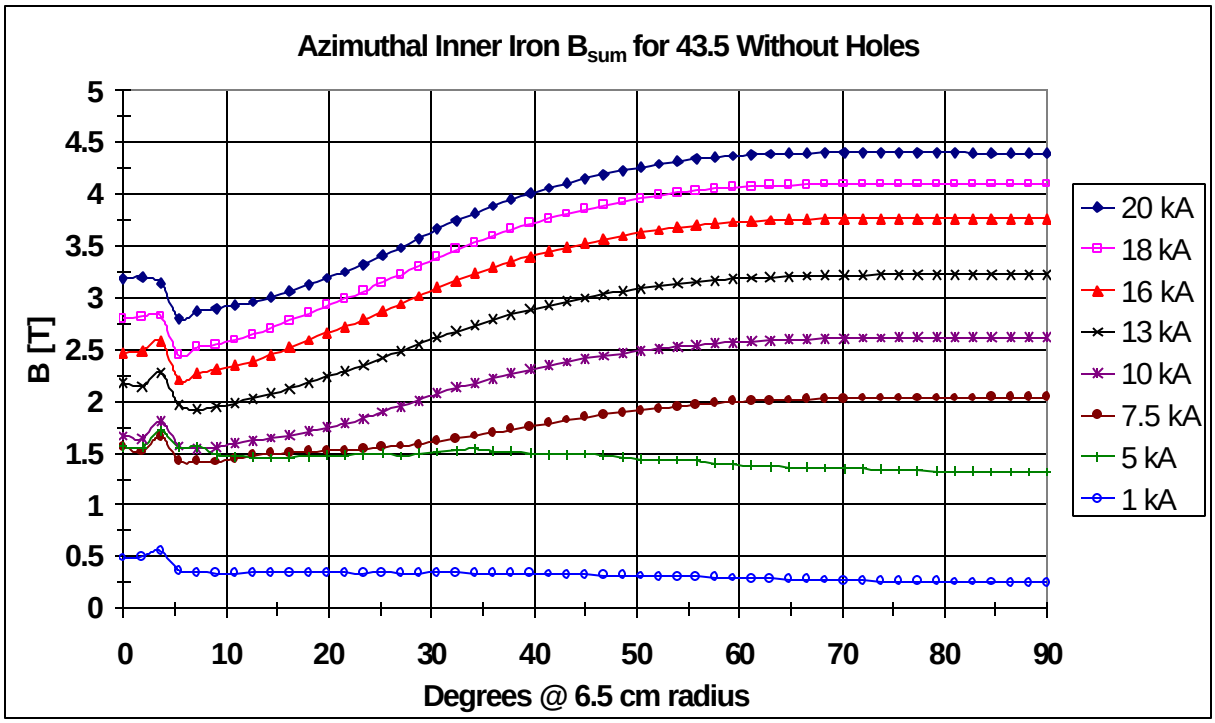

Figure 16. Magnetic flux density distribution taken azimuthally at 5-mm offset from inner radius of iron yoke for the finalized yoke design without holes.